

Search for galactic axions with a traveling wave parametric amplifier

R. Di Vora, A. Lombardi, A. Ortolan, R. Pengo, and G. Ruoso*
INFN, Laboratori Nazionali di Legnaro, 35020 Legnaro (Padova), Italy

C. Braggio
*INFN, Sezione di Padova, 35100 Padova, Italy and
 Dipartimento di Fisica e Astronomia, 35100 Padova, Italy*

G. Carugno and L. Taffarelo
INFN, Sezione di Padova, I-35100 Padova, Italy

G. Cappelli, N. Crescini, M. Esposito,[†] L. Planat, A. Ranadive, and N. Roch
Univ. Grenoble Alpes, CNRS, Grenoble INP, Institut Néel, 38000 Grenoble, France

D. Alesini, D. Babusci, A. D'Elia, D. Di Gioacchino, C. Gatti, C. Ligi, G. Maccarrone, A. Rettaroli, and S. Tocci
INFN, Laboratori Nazionali di Frascati, 00044 Frascati (Roma), Italy

D. D'Agostino, U. Gambardella, and G. Iannone
*Dipartimento di Fisica E.R. Caianiello, 84084 Fisciano (Salerno), Italy and
 INFN, Sezione di Napoli, 80126 Napoli, Italy*

P. Falferi
*Istituto di Fotonica e Nanotecnologie, CNR Fondazione Bruno Kessler, I-38123 Povo, Trento, Italy and
 INFN, TIFPA, 38123 Povo (Trento), Italy*

(QUAX Collaboration)
 (Dated: April 18, 2023)

A traveling wave parametric amplifier has been integrated in the haloscope of the QUAX experiment. A search for dark matter axions has been performed with a high Q dielectric cavity immersed in a 8 T magnetic field and read by a detection chain having a system noise temperature of about 2.1 K at the frequency of 10.353 GHz. Scanning has been conducted by varying the cavity frequency using sapphire rods immersed into the cavity. At multiple operating frequencies, the sensitivity of the instrument was at the level of viable axion models.

I. INTRODUCTION

The axion is an hypothetical particle that arises from the spontaneous breaking of the Peccei-Quinn symmetry of quantum chromodynamics (QCD), introduced to solve the so-called strong CP problem [1–3]. It is a pseudoscalar neutral particle having negligible interaction with the ordinary matter, making it a favourable candidate as a main component of dark matter [4]. Cosmological and astrophysical considerations suggest an axion mass range $1 \mu\text{eV} < m_a < 10 \text{ meV}$ [5].

The hunt for axions is now world spread and most of the experiments involved in this search use detectors based on the haloscope design proposed by Sikivie [6, 7]. Among them are ADMX [8–11], HAYSTAC [12, 13], ORGAN [14, 15], CAPP-8T [16, 17], CAPP-9T [18], CAPP-PACE [19], CAPP-18T [20], CAST - CAPP [21], CAPP-12TB [22], GrAHal [23], RADES [24–26], TASEH [27],

QUAX [28–33], and KLASH [34, 35]. Dielectric and plasma haloscopes have also been proposed, the most notable examples being MADMAX [36, 37] and ALPHA [38–40], respectively. The haloscope concept is based on the immersion of a resonant cavity in a strong magnetic field in order to stimulate the inverse Primakoff effect, converting an axion into an observable photon [41]. To maximise the power of the converted axion, the cavity resonance frequency has to be tuned to match the axion mass, while larger cavity quality factors Q will result in larger signals. Different solutions have been adopted to maximize the signal-to-noise ratio, facing the problem from different angles. Resonant cavities of superconductive and dielectric materials are becoming increasingly popular because of their high Q [42–45]. In this work we describe the results achieved by the haloscope of the QUAX- $a\gamma$ experiment, based on a high- Q dielectric cavity immersed in a static magnetic field of 8 T. Cooling of the cavity at $\sim 100 \text{ mK}$ reduces thermal fluctuations and enables operation of a traveling wave parametric amplifier (TWPA) at about the quantum limit. This is the first example of a high frequency haloscope (above 10 GHz) instrumented with a near quantum limited wide-band amplifier. A key step in the realization of an ap-

* Corresponding author: Giuseppe.Ruoso@lnl.infn.it

[†] Present address: CNR-SPIN Complesso di Monte S. Angelo, 80126 Napoli, Italy

NbTi superconducting wire (0.8 mm diameter) wound on an Aluminium reel. The inner diameter of this winding is 77.8 mm and its height is 250 mm. The counter field winding is biased in series to the main 8 T magnet, so it is able to reduce the field in the volume occupied by the TWPA, at any field strength, to a mean value of 0.04 T. To shield such remaining field a hybrid box encapsulates the two circulators C1 and C2 and the TWPA. This hybrid box is constituted by an external box of lead and an internal one of CRYOPERM®. The box dimension is $35 \times 65 \times 210 \text{ mm}^3$, with one small base opened to allow cabling, and is thermally anchored to the DU mixing chamber.

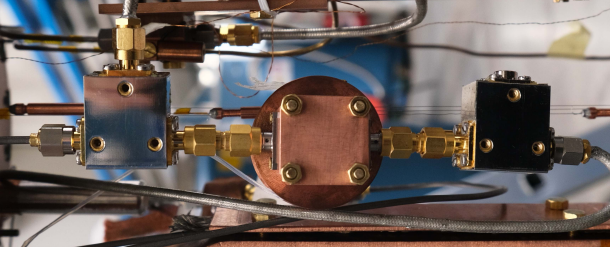


FIG. 3. Picture of the traveling wave parametric amplifier. The TWPA is enclosed in the central square box, the circle on the background is the holder of the superconducting coil providing the bias magnetic field. The two 3-port boxes are isolator C2 (on the right) and circulator C1 (on the left).

3. Amplifier characterization

The TWPA, see Figure 3, has been characterised following the procedure described in Ref. [49]. In particular its working point in terms of bias current I_b , frequency f_P and power A_P of the PUMP generator of Figure 2, has been chosen in order to minimize the system noise temperature T_{sys} at the cavity unshifted frequency ν_c . The performances of the TWPA have been measured several times with the magnetic field off, and then with the magnet energized once to 4 T and once to 8 T. All the resulting values of T_{sys} are compatible, around 2.0 K. During the magnet current ramp up we monitored the wide bandwidth gain of the amplifier, to look for possible variations of the working point induced by the stray field passing through the shielding. Since no changes have been observed, one can conclude that the residual field is much below one flux quanta. The wide bandwidth gain of the amplifier is shown in Figure 4(a). The PUMP frequency is set to $f_P = 9.4181 \text{ GHz}$, with $A_P = -16.5 \text{ dBm}$, and $I_b = -1.38 \text{ mA}$. It is evident from the figure that large (10 dB) oscillations of the gain are present at frequencies corresponding to higher gain. By precisely varying bias and PUMP frequency it is possible to align a gain maximum to the cavity frequency: a gain maximum is normally equivalent to a minimum system noise temperature. Figure 4(b) shows the gain in a 4 MHz in-

terval centred at the cavity resonant frequency. The two gain profiles are obtained with two different values of bias I_b : different values of bias set different working points for the TWPA, with corresponding different gain value and profile. In general higher gains means a much sharper gain profile, but even for the sharpest one a useful region of flat gain of about 1 MHz is obtained.

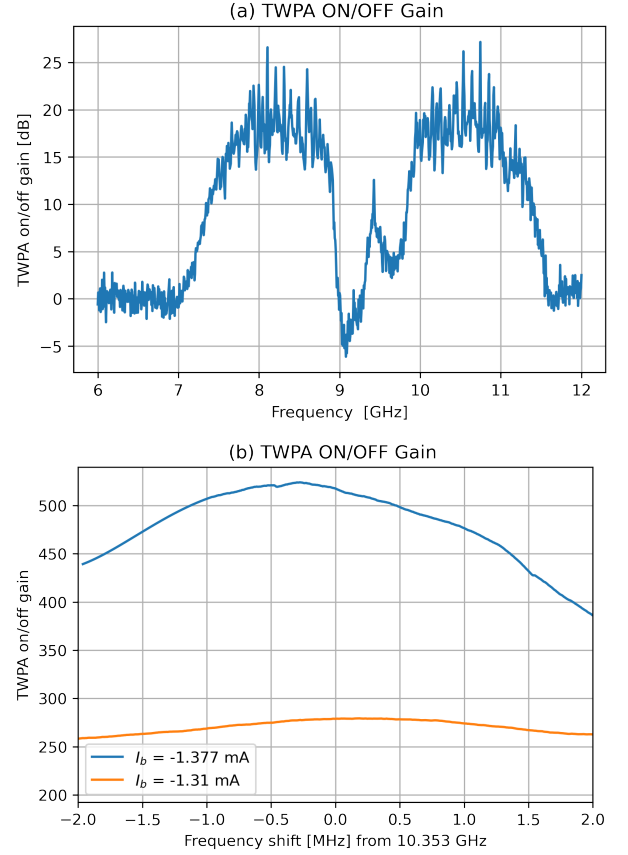


FIG. 4. Wide (a) and small (b) bandwidth gain of the traveling wave parametric amplifier. The gain has been estimated by the changes in transmission between the two cases PUMP ON and PUMP OFF [49]. (b) the two curves have been obtained with two different values of bias I_b on the TWPA.

n	Magnetic field (T)	Cavity Temp. (K)	T_{sys} (K) On Res.	K3 Temp. (K)	T_{sys} (K) Off Res.
1	0	0.12	2.12 ± 0.05	0.18	2.22 ± 0.06
2	0	0.12	2.04 ± 0.03	0.19	1.94 ± 0.03
3	4.0	0.13	2.11 ± 0.03	0.22	2.16 ± 0.03
4	0	0.12	1.89 ± 0.04	0.18	1.98 ± 0.05
5	8.0	0.11	2.23 ± 0.06	0.18	2.26 ± 0.06

TABLE I. Summary of measurement of system noise temperature T_{sys} at the cavity main frequency $\nu_c \simeq 10.353 \text{ GHz}$. "Res." stands for Resonance and "Temp." for Temperature.

Table I shows the measured values of system noise temperatures, all of them measured at the test frequency $\nu_c = 10.353 \text{ GHz}$. The table shows cavity and attenua-

tor temperatures, which contribute in different ways to the noise: the off cavity resonance value refers to a frequency 1 MHz detuned by ν_c , where only the attenuator noise is seen by the TWPA, while on resonance a combination between cavity noise and attenuator noise forms the input noise. Only for the case of critical coupling ($\beta = 1$), the noise at the cavity frequency is determined only by the cavity temperature. Except for the case $n=5$ (Magnetic field 8 T), having $\beta \simeq 22$, the other measurements have $\beta \simeq 3$. One extra measurement has been done at the frequency $\nu_{c,2} = 9.404061$ GHz, where another cavity mode is present. For such measurement the PUMP frequency was set to $f_{P,2} = 8$ GHz, for a resulting $T_{\text{sys}}(\nu_{c,2}) = 2.1 \pm 0.1$ K.

For the selected cavity mode TM030, the average value is $T_{\text{sys}}^{\text{avg}} = 2.06 \pm 0.13$ K on resonance, and $T_{\text{sys}}^{\text{avg}} = 2.07 \pm 0.14$ K off resonance. The central values come from the weighted average, while their errors are the standard deviation of all the values, showing a much wider distribution compared with the error of the single values. The resulting gain for the detection chain, from point A1 in Figure 1 to point P4 in Figure 2 is 74.7 ± 0.1 dB. We have also obtained the gains for the other two rf lines, resulting in -61.3 ± 0.1 dB from point P1 to A1, and -50.9 ± 0.1 dB from point P3 to A1. All these gain values are those in the presence of magnetic field at 8 T.

We can try now to evaluate all the various contributions to the measured noise level. In the quantum regime ($k_B T \ll h\nu$), the number of noise photons at frequency ν emitted by a thermal source is given by

$$N(\nu, T) = \frac{1}{2} \coth\left(\frac{h\nu}{2k_B T}\right), \quad (1)$$

where h is Planck constant, k_B is Boltzmann constant, T is a thermodynamic temperature. At the considered temperatures, the noise is entirely due to quantum fluctuations, as the contribution of the thermal photons is negligible.

At a given signal frequency ν_s , the noise power spectral density at the output of the HEMT amplifier is

$$\begin{aligned} \text{PSD}_{\text{HEMT}}(\nu_s) = & G_{\text{HEMT}} [N_{\text{HEMT}} + (1 - \Lambda_2) N_2 + \\ & \Lambda_2 G_{\text{TWPA}} (N_{\text{TWPA}} + (1 - \Lambda_1) N_1 + \\ & \Lambda_1 N(\nu_s, T_s) + \Lambda_1 N(\nu_i, T_i))] h\nu_s \end{aligned} \quad (2)$$

where G_{TWPA} is the net gain of the TWPA, N_{TWPA} and N_{HEMT} are the added noise of the TWPA and HEMT, respectively. $\Lambda_1 < 1$ is the transmission of the lossy chain from point A1 to the TWPA and, analogously, $\Lambda_2 < 1$ is the transmission from the output of the TWPA to the HEMT; N_1 and N_2 are the noise contributions coming from a simple beam splitter model for a lossy element.

$N(\nu_s, T_s)$ and $N(\nu_i, T_i)$ represent the quantum noise contributions at the signal frequency equal to the cavity frequency, $\nu_s = \nu_c$, and at the idler frequency, $\nu_i = 2f_P - \nu_c$, respectively[49]. At the idler frequency

the noise source is the attenuator K3, whose temperature is measured by one of the two thermometers. Its temperature has actually to be increased by the power leakage coming from the 4 K and room temperature stages. Considering the attenuation of K2 and K3 and cabling losses, we added 40 mK to the thermodynamic temperature of K3. At the signal frequency, the effective temperature is an intermediate value between the cavity temperature and the temperature of K3, the exact value depending on the coupling β : for $\beta = 1$ we have just the cavity temperature.

The line transmissions are estimated at room temperature for the non-superconducting cabling, resulting in $\Lambda_1 \simeq -0.3$ dB and $\Lambda_2 \simeq -0.7$ dB, which in linear units are close to 1. Such transmissions show low losses for the lines and allowed us to neglect the noise contributions N_1 and N_2 in Equation (2). In addition, the high gain of the HEMT allows us to neglect all the noise contribution entering after its amplification.

With such simplifications, Eq. (2) can be recast to estimate the total system noise (referred at the point A1),

$$\text{PSD}_{A1}(\nu_s) = \frac{\text{PSD}_{\text{HEMT}}(\nu_s)}{\Lambda_1 \Lambda_2 G_{\text{TWPA}} G_{\text{HEMT}}} = N_{\text{sys}} h\nu_s, \quad (3)$$

where we have defined N_{sys} as the total number of noise photons for the system, obtaining

$$N_{\text{sys}} \simeq N(\nu_s, T_s) + N(\nu_i, T_i) + \frac{N_{\text{TWPA}}}{\Lambda_1} + \frac{N_{\text{HEMT}}}{\Lambda_1 \Lambda_2 G_{\text{TWPA}}}. \quad (4)$$

Giving the measured value $T_{\text{sys}} = 2.06 \pm 0.13$ K, we obtain in terms of photons a noise level:

$$N_{\text{sys}} = \frac{k_B}{h\nu_s} T_{\text{sys}} = 4.2 \pm 0.3. \quad (5)$$

Term	Value (K)	N photons
$N(\nu_s, T_s)$	0.27	0.5
$N(\nu_i, T_i)$	0.27	0.7
$N_{\text{HEMT}}/\Lambda_1 \Lambda_2 G_{\text{TWPA}}$	0.39	0.8
N_{sys}	2.06	4.2
$N_{\text{TWPA}}/\Lambda_1$		2.2

TABLE II. Noise contributions to the system noise. In the column Value, the noise is expressed in terms of Equivalent Noise Temperature. The following values have been used: $\nu_s = 10.353$ GHz, $\nu_i = 7.94$ GHz, and the thermodynamic temperatures $T_s = 0.16$ K, $T_i = 0.22$ K. $N_{\text{TWPA}}/\Lambda_1$ is the difference between the measured N_{sys} and the sum of the preceding terms.

In order to disentangle the contribution of the HEMT, we measured the system noise with the TWPA off (with PUMP OFF and without bias). The resulting noise temperature in this case was 49 ± 1 K, with a total gain reduced by a factor 125. The contribution of the HEMT to the total noise temperature is then 0.39 ± 0.01 K. Table II summarises the noise contributions and allows to derive the TWPA added noise as $N_{\text{TWPA}} \simeq 2.1$ photons at the frequency of 10.353 GHz.

4. Data taking

RUN n	ν_c (GHz)	Duration (s)	T_c (mK)	T_{K3} (mK)
389	10.353 525	2000	113	177
392	10.353 499	2000	111	178
394	10.353 473	2000	112	181
395	10.353 473	4000	113	185
397	10.353 444	2000	114	182
399	10.353 424	4800	112	177
401	10.353 399	28000	110	176
404	10.353 368	2000	110	176

TABLE III. Summary of the RUNs performed for the axion dark matter search. The cavity frequency is the value determined via a fast tracking spectrum on the SA. The frequency of the LO has been set to 10.353 GHz for all RUNs but RUN 404, where it is set to 10.3529 GHz. T_c and T_{K3} are the cavity and attenuator K3 temperatures, respectively.

The search for axion dark matter has been performed over a time span of about 17 consecutive hours. The cavity antenna coupling has been set to overcritical, with the target to have a loaded quality factor about 4 times smaller than the axion one[50]. This is important for what concern data analysis. Data taking is divided in different units that we usually call RUN, each RUN differing from another normally for the cavity central frequency that can be varied with the sapphire triplets described above. The detection chain system noise temperature and gain have been measured once at the beginning of the scanning session, and we monitored the time stability of the gain by injecting a rf pure tone of amplitude -90 dBm on line L3 using SG2 at a frequency 900 kHz above the LO frequency. The LO frequency is chosen in order to keep the cavity frequency in a central band of the ADC working region. Each data taking step is composed of the following actions:

- action 1:** Set the cavity frequency to the desired value by moving the sapphire triplets. Set the LO frequency: this is actually not done for every step, since normally the change in cavity frequency is much smaller of the ADC bandwidth.
- action 2:** Measure a cavity reflection spectrum by tracking generator SG2 with the spectrum analyser SA. Data are saved on a file to be fitted to deduce the antenna coupling β .
- action 3:** Measure a cavity transmission spectrum by using the noise source on line L1 and acquiring data with the ADC. Data are also taken with the the spectrum analyser SA for quick analysis. The number of 4 s blocks acquired with the ADC is normally about 30.
- action 4:** Measure the cavity output with all the inputs off, acquiring data with the ADC. This is the axion search data, and normally we collect 500 blocks of

4 s length each. Some RUNs have been done with a larger number of blocks. Again, data are also taken with the the spectrum analyser SA for quick analysis.

Table III summarizes all the scans performed. Figure 5 shows all the vacuum spectra measured with the spectrum analyser. Such plots are only taken for control purpose, while the data sampled by the ADC and stored in the computer are those used for the search and will be discussed in Section III.

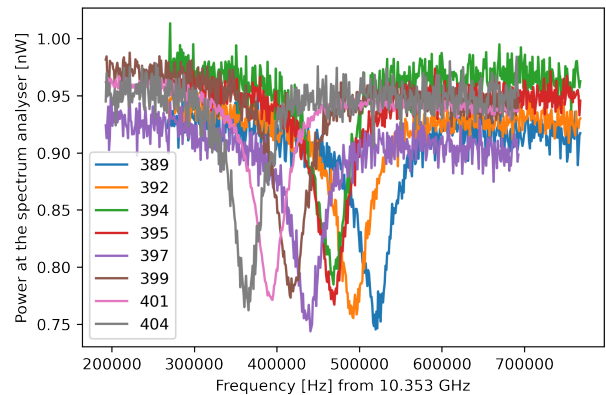


FIG. 5. Cumulative plots of the axion search measurements with the magnet energized (action 4). Such plots are taken using the spectrum analyser, i.e. at the point P4 of Figure 2, only for control purpose during data taking and are not used in the data analysis. The different levels outside the resonance is a measure of the gain stability of the system, kept within a few percent in a 17 hours time span. The resolution bandwidth for these plots is 1 kHz. Different colors refer to the different RUNs.

5. Raw data processing

The 4 s long time sequences produced by the ADC are divided into chunks about 1.5 ms long, which are Fourier transformed and averaged. Another averaging is then performed to obtain a single power spectrum PS_n for each RUN having a resolution of $B = 651$ Hz and covering the down converted window $[-1, +1]$ MHz. A raw data processing is performed to obtain relevant parameters. This is the same procedure already described in [30]. In particular, the antenna coupling β is obtained by fitting the cavity reflection spectrum measured with the spectrum analyser SA with tracking generator SG2 (see 'action 2'). The cavity loaded quality factor Q_L and central frequency ν_c are obtained by fitting the average spectra obtained from the ADC data collected while the diode noise source was at the input of line L1 (see 'action 3'). The resulting parameters are reported in Table IV. The table reports also the amplitude of the reference peak set to the frequency +900 kHz in the down converted spectra. This measurement shows again that

the stability of the detection chain gain was within a few percent along the complete data taking.

RUN n	$\nu_c - 10.353$ GHz (Hz)	Cavity Q_L	β	Ref Peak (a.u.)
389	522 600	230 000	21.6	179
392	494 100	240 000	23.8	185
394	468 800	245 000	24.2	186
395	468 800	245 000	24.2	187
397	439 800	245 000	22.7	175
399	418 500	245 000	22.6	191
401	393 100	250 000	22.5	186
404	365 400	255 000	23.5	193

TABLE IV. Summary of the parameters obtained by the fits of preliminary data for all the RUNs performed. Ref Peak is the amplitude of the reference peak due to the pure tone injected by SG2 on line L3 during data taking at a frequency 900 kHz above the reference oscillator of the mixer. The fits errors on the values of cavity frequencies are about 100 Hz, for the loaded quality factors about 3000, and for the β 's about 0.2.

During the raw analysis, a careful check of the ADC data compared with the SA data has evidenced a problem present in the down-converted data. The ADC input is filtered by a single pole low pass filter having the -3 dB point at about 1.7 MHz. Unfortunately this is not enough to avoid aliasing of the rather flat noise input. From the comparison of the high frequency and down converted spectra we estimate that the measured wide band noise is about a factor 1.7 larger with respect to the real average noise in the vicinity of the cavity resonance.

Each power spectrum PS_n is the readout of the ADC input, and to obtain the power at the cavity output it must be divided by the overall gain. Alternatively, one equals the noise level measured at the ADC with the power given by the effective noise temperature of the system. We have assumed that the system noise temperature has not changed over the entire data taking time, having a duration of 17 hours. Indeed, the relative error of the T_{sys} , about 6.3 %, is larger of the relative changes of the reference peak as obtained by Table IV having a maximum of 5.1 %. For each RUN we assume that the noise level at the cavity frequency is

$$P_n(\nu) = k_B T_{\text{sys}}^{\text{ADC}} B \quad (6)$$

where $B = 651$ Hz is the bin width, k_B is the Boltzmann's constant, and $T_{\text{sys}}^{\text{ADC}} = 1.7 \times T_{\text{sys}} = 3.5$ K.

III. DATA ANALYSIS AND RESULTS

A. Axion Detection procedure

Detection algorithms can be discussed in the classical "hypothesis testing" framework: on the basis of the observed data, we must decide whether to reject or fail to reject the null hypothesis (data are consistent with

noise) against the alternative hypothesis (noise and signal are present in data) usually by means of a detection threshold determined by the desired significance level. The outcome of this data analysis step is a set of "axion candidate" masses or frequencies. However, axion signal has some distinctive properties that can be used to discriminate it from spurious detected signals (see Sect. III.B). We emphasize that the basis of our detection algorithm is a very robust model of the noise that allow us to use maximum likelihood criterion (i.e. a χ^2 test) to implement the decision rule. Deviations from the model of the noise power spectral density are clues of excess power that could be associated with a signal. In the frequency domain, the noise model for the power spectral density at the haloscope output (under the general assumptions of linearity, stationarity, ergodicity and single-resonance system) is simply a first order polynomial ratio

$$p(\nu) = \frac{\nu - \nu_z + i\gamma_z}{\nu - \nu_p + i\gamma_p} \quad (7)$$

where $(\nu - \nu_{p,z} + i\gamma_{p,z})$ are the pole and the zero values in the complex plane, respectively. The fitting function to the power spectrum data, with fit parameters a, b, \dots, f , reads

$$F(\nu) = e^2 * \frac{|\nu - a + ib|^2}{|\nu - c + id|^2} + f * (\nu - c) \quad (8)$$

where the linear term accounts for the slight dependence of the ADC gain on frequency and we made the approximation $\nu^2 - \nu_{p,z}^2 \simeq 2\nu_{p,z}(\nu - \nu_{p,z})$. The parameter e is a normalization factor.

The estimate of power spectrum resides on the Bartlett method of averaging periodograms [51]. For every measured RUN of table III we performed the fit with $F(\nu)$ and used the χ^2 to test the hypothesis of no signal. We discovered that the quality, i.e. the value for example of the reduced χ^2 , of the fits was worsening with the duration of the RUN. Indeed, a key issue is the stability of our set-up, where it is actually not surprisingly that drifts will appear over time scales of several hours. For this reason we decided, for the analysis procedure, to split every RUN in subruns with a fixed length of 2000 s, and to perform the fits on each of the resulting 23 subruns. For each subrun, the fits are performed on a window of 200 bins (bin width = 651 Hz) centered at the cavity peak frequency. The weight on each bin is the measured value divided by \sqrt{N} , N is the number of averages: for a 2000 s duration and 651 Hz bin width, $N \simeq 1.37 \cdot 10^6$. The null hypothesis H_0 is accepted for χ^2 probability above the chosen threshold of $P_\alpha = 0.001$. Since for all subruns H_0 was not rejected, it is then possible to build a grand spectrum of all the residuals of the different fits, which will result in an increased sensitivity.

The grand spectrum is built by performing a weighted average of all the bins with the same frequency for all subruns residuals, again using as weight the values previously used to do the fits. The grand spectrum of the residuals

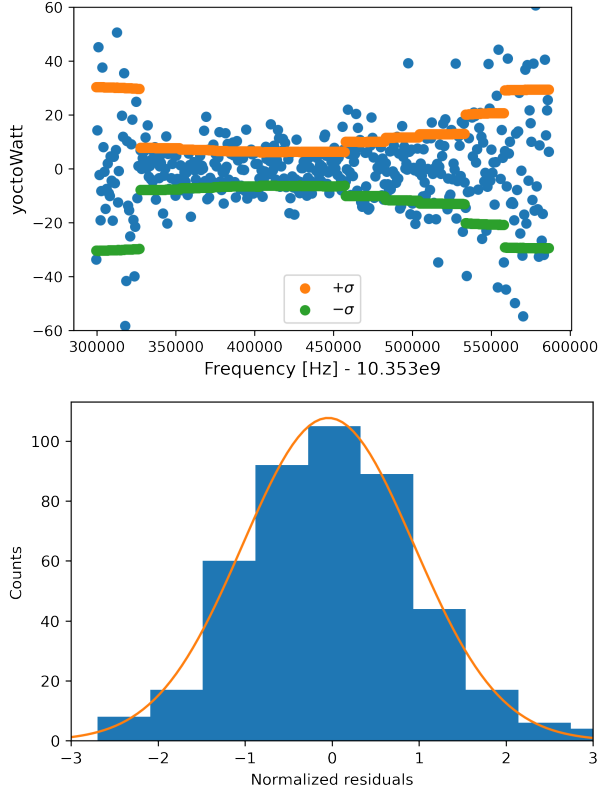


FIG. 6. Grand spectrum of the residuals. (a) Residuals and their sigma versus frequency. The bin size is 651 Hz. (b) Histogram of the normalized residuals. The fit function is a gaussian function with average -0.04 and width 0.99.

and the relative histograms of the normalized values are shown in Figure 6. The grand spectrum has 442 bins, a total $\chi^2 = 452$ having a probability $P_{\chi^2} = 0.37$, and the hypothesis of data compatible with pure thermal noise is not rejected. Such a claim is done without modeling the axion. The minimum value of the sigma of the residuals in Figure 6 is $(6.2 \pm 0.4) \cdot 10^{-24}$ W, obtained at the frequency of 403645 Hz shifted from 10.353 GHz with a total integration time of 36000 s. The value expected from Dicke's radiometer equation is $(6.5 \pm 0.4) \cdot 10^{-24}$ W.

B. Axion Discrimination procedures

Candidates that survive to a simple repetition of the χ^2 test (using a new data set taken in the same experimental conditions) can be further discriminated using a stationarity and on-off resonance tests. A stationarity test verifies that a signal is continuously present during a data taking. An on-off resonance test verifies that the signal can be maximized by a tuning procedure of the cavity. Moreover, the dependence of signal power on the antenna coupling β can also be checked. Eventually, a change of the magnetic field allow us to verify if the signal power is proportional to the magnetic field squared.

Candidates that passed this step would be associated to axionic dark matter. When no axion candidate survive at the sensitivity level of current axion models[52], an upper limit on axion-photon coupling can be set for the standard model of Galaxy halo.

C. Upper limits on axion-photon coupling

Having data compatible with the presence of only noise, we can then proceed to derive bounds on the coupling constant of the axion to the photon, assuming specific coupling and galactic halo models. Bounds can be inferred adopting the following approach. The power spectra for each subrun are fitted again using as fit function the sum of the background $F(\nu)$ (see Equation (8)) and the expected power produced by axion conversion for specific values of the axion mass within the measured bandwidth. By placing the axion coupling as a free parameter, since this new fit procedure returns as output the smallest possible observable power, it is possible to obtain an upper limit on the coupling constant $g_{a\gamma\gamma}$. Again, χ^2 probability is used to evaluate the goodness of the fit.

To calculate the expected axion signal we will rely on the standard halo model for dark matter, and assume that dark matter is composed by axions in its totality. With this hypothesis, the axion energy distribution is given by a Maxwell-Boltzman distribution [50]

$$f_a(\nu, \nu_a) = \frac{2}{\sqrt{\pi}} \sqrt{\nu - \nu_a} \left(\frac{3}{1.7 \nu_a \langle \beta_a^2 \rangle} \right)^{3/2} e^{-\frac{3(\nu - \nu_a)}{1.7 \nu_a \langle \beta_a^2 \rangle}} \quad (9)$$

where ν_a is the axion frequency and $\langle \beta_a^2 \rangle$ is the RMS of the axion velocity distribution normalized by the speed of light. The factor 1.7 takes into account that we are working in the laboratory frame [53]. The RMS of the galactic halo is 270 km/s, resulting in a $\langle \beta_a^2 \rangle$ of $8.1 \cdot 10^{-7}$.

In a haloscope, the power is released in a microwave cavity of frequency ν_c and volume V , immersed in a static magnetic field B_0 . At the antenna output, with coupling β , the available power is described by the spectrum

$$S_a(\nu, \nu_a, \nu_c) = g_{a\gamma\gamma}^2 \frac{\hbar^3 c^3 \rho_a}{m_a^2} \times \times \frac{2\pi\nu_c B_0^2 V C_{030}}{\mu_0} \frac{\beta}{1 + \beta} \cdot F_c(\nu, \nu_c) \cdot f_a(\nu, \nu_a) \quad (10)$$

where $\rho_a \sim 0.45 \text{ GeV/cm}^3$ is the local dark matter density [54], $g_{a\gamma\gamma}$ is the coupling constant of the axion-photon interaction, m_a is the axion mass. The form factor $C_{030} = 0.035$ has been recalculated to take into account the static magnetic field distribution over the cavity mode TM030 used in our haloscope. The function

$$F_c(\nu, \nu_c) = \frac{Q_L}{1 + \left[2Q_L \frac{(\nu - \nu_c)}{\nu_c} \right]^2} \quad (11)$$

describes the bandwidth limited amplification of the microwave cavity, with Q_L its loaded quality factor.

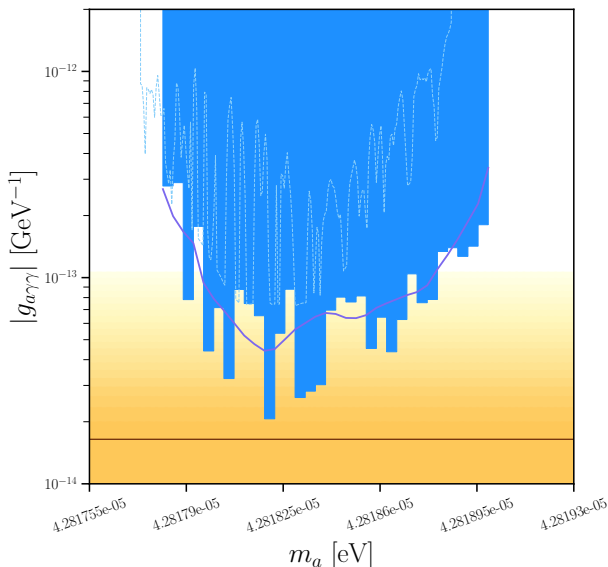


FIG. 7. $g_{a\gamma\gamma}$ axion coupling constant upper limit calculated with 90% single-sided C.L. as a function of the axion mass. The solid blue bars are the limits obtained with the data and the analysis described in this manuscript. The solid dark blue line is the expected limit in the case of no signal. The dashed light blue line are the limits obtained in our previous work [30]. The yellow region indicates the QCD axion model band. The horizontal line shows the theoretical prediction for the coupling constant given by the KSVZ[55, 56] model. Image realized with [57].

We split the measured frequency range in 33 intervals having center frequencies ν_i , where we tested our sensitivity for an axion of mass $m_a = h\nu_i/c^2$ in order to obtain limits on its coupling. By using the discretized function:

$$W(\nu_i, \nu_a, \nu_c) = F(\nu_i) + S_s(\nu_i, \nu_a, \nu_c)B \quad (12)$$

fits were performed on all the 23 subruns. This fit function has $g_{a\gamma\gamma}^2$ as fitting parameter, in addition to those of $F(\nu)$ previously described. In order for the fits to converge, the parameters of $F(\nu)$ have as initial guess the values found when fitting only the background and they are also constrained to vary in a small interval. We have verified that such procedure is able to extract the correct value of $g_{a\gamma\gamma}^2$ by performing Monte Carlo simulations with software injected signals in our data.

The 23 estimated set of values $g_{a\gamma\gamma}^2(\nu_i)$ are then averaged using as weights the inverse of their squared uncertainties extracted by the fitting procedure. Using this approach we are able to extract a set of $g_{a\gamma\gamma}^2$ values from which we calculated the limit on the coupling strength with a 90% confidence level [29], adopting a power constrained procedure for the values of $g_{a\gamma\gamma}^2$ that fluctuates below $-\sigma_{g_{a\gamma\gamma}}$ [58]. The upper limit $g_{a\gamma\gamma}^{\text{CL}}$ obtained adopting this procedure in the axion mass

range $42.8178 - 42.8190 \mu\text{eV}$ are reported in Figure 7 as blue bars. The minimum value sets a limit $g_{a\gamma\gamma}^{\text{CL}} < 2.05 \cdot 10^{-14} \text{ GeV}^{-1}$, that is 1.2 times larger respect to the benchmark KSVZ axion models [55, 56].

IV. CONCLUSIONS

We reported results of the search of galactic axions using an high-Q dielectric haloscope instrumented with a detection chain based on a traveling wave parametric amplifier working close to the quantum limit. The investigated mass range is $42.8178 - 42.8190 \mu\text{eV}$, partially already investigated by us in a previous run and not currently accessible by other experiments. We set a limit to the axion coupling constant that is about 1.2 times larger respect to the benchmark KSVZ axion model. Our results demonstrate the reliability of our approach, which complements high Q factor dielectric cavities with strong magnetic field, and operation in ultra-cryogenic environment to exploit the noise performances of the TWPA based detection chain. This is the first time a wide bandwidth quantum limited amplifier has been used in a haloscope working at high frequency, where internal losses of the components are significantly larger with respect to frequencies in the lower octave band. A result that complements the one obtained at 5 GHz by the ADMX collaboration [59], and paves the road for the exploration of the axion mass parameter space at frequencies above 10 GHz.

This result improves a factor about 4 the sensitivity we obtained in our previous run in almost the same frequency range, thanks to the new amplifier and an improved description of the background in the data analysis, based on a robust noise model. With the implementation of anti-aliasing filters in our digitizing channels and a planned better isolation of the first stage amplifier, we expect to improve even more our sensitivity in the next run. A new type of cavity with larger effective volume and larger tuning will be put in operation for a future campaign of axion searches capable of covering a sizable range of mass values in the 40's μeV range.

ACKNOWLEDGMENTS

We are grateful to E. Berto, A. Benato, and M. Rebeschini for the mechanical work; F. Calao and M. Tesaro for help with the electronics and cryogenics. We thank G. Galet and L. Castellani for the development of the magnet power supply, and M. Zago who realized the technical drawings of the system. We deeply acknowledge the Cryogenic Service of the Laboratori Nazionali di Legnaro for providing us with large quantities of liquid helium on demand.

This work is supported by INFN (QUAX experiment), by the U.S. Department of Energy, Office of Science,

National Quantum Information Science Research Centers, Superconducting Quantum Materials and Systems Center (SQMS) under the Contract No. DE-AC02-07CH11359, by the European Union’s FET Open SUPERGALAX project, Grant N.863313 and by the European Union’s Horizon 2020 research and innovation program under grant agreement no. 899561. M.E. acknowledges the European Union’s Horizon 2020 research and innovation program under the Marie Skłodowska Curie (grant agreement no. MSCA-IF-835791). A.R. acknowledges the European Union’s Horizon 2020 research and innovation program under the Marie Skłodowska Curie grant agreement No 754303 and the ‘Investissements

d’avenir’ (ANR-15- IDEX-02) programs of the French National Research Agency. N.C. is supported by the European Union’s Horizon 2020 research and innovation program under the Marie Skłodowska-Curie grant agreement QMET No. 101029189.

The data that support the findings of this study are available from the corresponding author upon reasonable request.

Appendix: Details on the experimental set up

Table V shows the relevant components used in the experimental set-up.

-
- [1] S. Weinberg, A new light boson?, *Phys. Rev. Lett.* **40**, 223 (1978).
 - [2] F. Wilczek, Problem of strong p and t invariance in the presence of instantons, *Phys. Rev. Lett.* **40**, 279 (1978).
 - [3] R. D. Peccei and H. R. Quinn, Cp conservation in the presence of pseudoparticles, *Phys. Rev. Lett.* **38**, 1440 (1977).
 - [4] J. Preskill, M. B. Wise, and F. Wilczek, Cosmology of the invisible axion, *Phys. Lett. B* **120**, 127 (1983).
 - [5] I. G. Irastorza and J. Redondo, New experimental approaches in the search for axion-like particles, *Prog. Part. Nucl. Phys.* **102**, 89 (2018).
 - [6] P. Sikivie, Experimental tests of the “invisible” axion, *Phys. Rev. Lett.* **51**, 1415 (1983).
 - [7] P. Sikivie, Detection rates for “invisible”-axion searches, *Phys. Rev. D* **32**, 2988 (1985).
 - [8] T. Braine, R. Cervantes, N. Crisosto, N. Du, S. Kimes, L. Rosenberg, G. Rybka, J. Yang, D. Bowring, A. Chou, *et al.*, Extended search for the invisible axion with the axion dark matter experiment, *Phys. Rev. Lett.* **124**, 101303 (2020).
 - [9] N. Du, N. Force, R. Khatiwada, E. Lentz, R. Ottens, L. Rosenberg, G. Rybka, G. Carosi, N. Woollett, D. Bowring, *et al.*, Search for invisible axion dark matter with the axion dark matter experiment, *Phys. Rev. Lett.* **120**, 151301 (2018).
 - [10] C. Boutan, M. Jones, B. H. LaRoque, N. Oblath, R. Cervantes, N. Du, N. Force, S. Kimes, R. Ottens, L. Rosenberg, *et al.*, Piezoelectrically tuned multimode cavity search for axion dark matter, *Phys. Rev. Lett.* **121**, 261302 (2018).
 - [11] C. Bartram *et al.*, *Phys. Rev. Lett.* **127**, 261803 (2021).
 - [12] K. M. Backes, D. A. Palken, S. A. Kenany, B. M. Brubaker, S. Cahn, A. Droster, G. C. Hilton, S. Ghosh, H. Jackson, S. K. Lamoreaux, *et al.*, A quantum enhanced search for dark matter axions, *Nature* **590**, 238 (2021).
 - [13] L. Zhong, S. Al Kenany, K. Backes, B. Brubaker, S. Cahn, G. Carosi, Y. Gurevich, W. Kindel, S. Lamoreaux, K. Lehnert, *et al.*, Results from phase 1 of the haystack microwave cavity axion experiment, *Phys. Rev. D* **97**, 092001 (2018).
 - [14] B. T. McAllister, G. Flower, E. N. Ivanov, M. Goryachev, J. Bourhill, and M. E. Tobar, The organ experiment: An axion haloscope above 15 ghz, *Phys. Dark Univ.* **18**, 67 (2017).
 - [15] A. Quiskamp, B. T. McAllister, P. Altin, E. N. Ivanov, M. Goryachev, and M. E. Tobar, Direct search for dark matter axions excluding alp cogenesis in the 63- to 67- μeV range with the organ experiment, *Science Advances* **8**, eabq3765 (2022).
 - [16] J. Choi, S. Ahn, B. Ko, S. Lee, and Y. K. Semertzidis, Capp-8tb: Axion dark matter search experiment around 6.7 μeV , *Nucl. Inst. Meth. Phys. Res. A* **1013**, 165667 (2021).
 - [17] S. Lee, S. Ahn, J. Choi, B. Ko, and Y. K. Semertzidis, Axion dark matter search around 6.7 μeV , *Phys. Rev. Lett.* **124**, 101802 (2020).
 - [18] J. Jeong, S. Youn, S. Bae, J. Kim, T. Seong, J. E. Kim, and Y. K. Semertzidis, Search for invisible axion dark matter with a multiple-cell haloscope, *Phys. Rev. Lett.* **125**, 221302 (2020).
 - [19] O. Kwon, D. Lee, W. Chung, D. Ahn, H. Byun, F. Caspers, H. Choi, J. Choi, Y. Chong, H. Jeong, *et al.*, First results from an axion haloscope at capp around 10.7 μeV , *Phys. Rev. Lett.* **126**, 191802 (2021).
 - [20] Y. Lee, B. Yang, H. Yoon, M. Ahn, H. Park, B. Min, D. Kim, and J. Yoo, Searching for invisible axion dark matter with an 18 t magnet haloscope, *Phys. Rev. Lett.* **128**, 241805 (2022).
 - [21] C. M. Adair, K. Altenmüller, V. Anastassopoulos, S. A. Cuendis, J. Baier, K. Barth, A. Belov, D. Bozicevic, H. Bräuninger, G. Cantatore, F. Caspers, J. F. Castel, S. A. Çetin, W. Chung, H. Choi, J. Choi, T. Dafni, M. Davenport, A. Dermenev, K. Desch, B. Döbrich, H. Fischer, W. Funk, J. Galan, A. Gardikiotis, S. Gninenko, J. Golm, M. D. Hasinoff, D. H. H. Hoffmann, D. D. Ibáñez, I. G. Irastorza, K. Jakovčić, J. Kaminski, M. Karuza, C. Krieger, Ç. Kutlu, B. Lakić, J. M. Laurent, J. Lee, S. Lee, G. Luzón, C. Malbrunot, C. Margalejo, M. Maroudas, L. Miceli, H. Mirallas, L. Obis, A. Özbey, K. Özbozdoğan, M. J. Pivovarov, M. Rosu, J. Ruz, E. Ruiz-Chóliz, S. Schmidt, M. Schumann, Y. K. Semertzidis, S. K. Solanki, L. Stewart, I. Tsagris, T. Vafeiadis, J. K. Vogel, M. Vretenar, S. Youn, and K. Zioutas, Search for dark matter axions with CAST-CAPP, *Nature Communications* **13**, 10.1038/s41467-022-33913-6 (2022).

Components	Type	Provider/Model	Parameters @ 10 GHz
Cryogenic set up - Figure 1			
K1, K2, K3	Attenuators	Hewlett Packard 8493B 20 DB	IL = 20 dB
C1	Circulator	Raditek RADC-8-12-Cryo-0.02-4K-S23-1WR-MS-b	IL = 0.6 dB
C2, C3	Isolator	Raditek RADI-8-12-Cryo-0.02-4K-S23-1WR-MS-b	IL = 0.6 dB
HP	High Pass Filter	Mini Circuit VHF-7150+	IL = 0.7 dB
Cables	RF Cable	KeyCom ULT-05	IL = 1.9 dB/m
Cables	SC RF Cable	KeyCom NbTiNbTi085	–
HEMT	Amplifier	Low Noise Factory LNF-LNC4-16B	Gain = 42 dB
①	Thermometer	ICE Oxford RuO2 RCWPM 1206-68-2.21 KOHM	
I_{DC}	Current source	Keithley 263	
Room temperature set up - Figure 2			
K4	Attenuator	Narda Micro-Pad 4779 - 12	IL = 12 dB
Cables	RF Cable	Huber - Suhner SF104	IL = 1 dB/m
CD1	Power Splitter	Macom 1147	
CD2	Power Combiner	Triangle Microwave YL - 74	
HEMT	Amplifier	Low Noise Factory LNF-LNR4-16B	Gain = 35 dB
AI, AQ	Amplifier	Femto DPHVA-101	Gain (1 MHz) = 50 dB
Mixer	Mixer	Miteq IRM0812LC2Q	–
A1	Amplifier	MITEQ AFS4-08001200-10-CR-4	Gain = 32 dB
Noise Source	Noise Source	Micronetics NS346B	$T_{eff} = 10000$ K
SG1, SG2, LO, PUMP	Signal Generator	Keysight N5183/N5173	
SA	Spectrum Analyser	Keysight N9010B	
ADC	Analog to digital Converter	National Instruments USB 6366	Rate = 2 Ms/s
Other components			
Dewar		Precision Cryogenics System Inc.	
Dilution Unit		Leiden Cryogenics	
Magnet		Cryogenic Ltd	

TABLE V. Description of the relevant components for the experimental setup. IL = Insertion Loss.

- [22] A. K. Yi, S. Ahn, i. m. c. b. u. Kutlu, J. Kim, B. R. Ko, B. I. Ivanov, H. Byun, A. F. van Loo, S. Park, J. Jeong, O. Kwon, Y. Nakamura, S. V. Uchaikin, J. Choi, S. Lee, M. Lee, Y. C. Shin, J. Kim, D. Lee, D. Ahn, S. Bae, J. Lee, Y. Kim, V. Gkika, K. W. Lee, S. Oh, T. Seong, D. Kim, W. Chung, A. Matlashov, S. Youn, and Y. K. Semertzidis, Axion dark matter search around $4.55 \mu\text{eV}$ with dine-fischler-srednicki-zhitnitskii sensitivity, *Phys. Rev. Lett.* **130**, 071002 (2023).
- [23] T. Grenet, R. Ballou, Q. Basto, K. Martineau, P. Perrier, P. Pugnat, J. Quevillon, N. Roch, and C. Smith, *arXiv:2110.14406* (2021).
- [24] A. Á. Melcón, S. A. Cuendis, C. Cogollos, A. Díaz-Morcillo, B. Döbrich, J. D. Gallego, J. Barceló, B. Gimeno, J. Golm, I. G. Irastorza, *et al.*, Scalable haloscopes for axion dark matter detection in the $30 \mu\text{eV}$ range with rades, *JHEP* **07** (2020), 084.
- [25] A. A. Melcon, S. A. Cuendis, C. Cogollos, A. Díaz-Morcillo, B. Döbrich, J. D. Gallego, B. Gimeno, I. G. Irastorza, A. J. Lozano-Guerrero, C. Malbrunot, *et al.*, Axion searches with microwave filters: the rades project, *JCAP* **05** (2018), 040.
- [26] A. Álvarez Melcón, S. Arguedas Cuendis, J. Baier, K. Barth, H. Bräuninger, S. Calatroni, G. Cantatore, F. Caspers, J. Castel, S. A. Cetin, *et al.*, First results of the cast-rades haloscope search for axions at $34.67 \mu\text{eV}$, *JHEP* **10** (2021), 075.
- [27] H. Chang, J.-Y. Chang, Y.-C. Chang, Y.-H. Chang, Y.-H. Chang, C.-H. Chen, C.-F. Chen, K.-Y. Chen, Y.-F. Chen, W.-Y. Chiang, W.-C. Chien, H. T. Doan, W.-C. Hung, W. Kuo, S.-B. Lai, H.-W. Liu, M.-W. OuYang, P.-I. Wu, and S.-S. Yu (TASEH Collaboration), Taiwan axion search experiment with haloscope: Cd102 analysis details, *Phys. Rev. D* **106**, 052002 (2022).
- [28] D. Alesini, C. Braggio, G. Carugno, N. Crescini, D. D'Agostino, D. Di Gioacchino, R. Di Vora, P. Falferi, S. Gallo, U. Gambardella, *et al.*, Galactic axions search with a superconducting resonant cavity, *Phys. Rev. D* **99**, 101101 (2019).
- [29] D. Alesini, C. Braggio, G. Carugno, N. Crescini, D. D'Agostino, D. Di Gioacchino, R. Di Vora, P. Falferi, U. Gambardella, C. Gatti, *et al.*, Search for invisible axion dark matter of mass $m_a = 43 \mu\text{eV}$ with the quax- α γ experiment, *Phys. Rev. D* **103**, 102004 (2021).
- [30] D. Alesini, D. Babusci, C. Braggio, G. Carugno, N. Crescini, D. D'Agostino, A. D'Elia, D. Di Gioacchino, R. Di Vora, P. Falferi, U. Gambardella, C. Gatti, G. Iannone, C. Ligi, A. Lombardi, G. Maccarrone, A. Ortolan, R. Pengo, A. Rettaroli, G. Ruoso, L. Taffarello, and S. Tocci, Search for galactic axions with a high- q dielectric cavity, *Phys. Rev. D* **106**, 052007 (2022).
- [31] R. Barbieri, C. Braggio, G. Carugno, C. S. Gallo, A. Lombardi, A. Ortolan, R. Pengo, G. Ruoso, and C. C. Speake, Searching for galactic axions through magnetized media: the quax proposal, *Phys. Dark Univ.* **15**, 135 (2017).
- [32] N. Crescini, D. Alesini, C. Braggio, G. Carugno, D. Di Gioacchino, C. Gallo, U. Gambardella, C. Gatti,

- G. Iannone, G. Lamanna, *et al.*, Operation of a ferromagnetic axion haloscope at $m_a = 58 \mu\text{eV}$, *Eur. Phys. J. C* **78**, 1 (2018).
- [33] N. Crescini, D. Alesini, C. Braggio, G. Carugno, D. D'Agostino, D. Di Gioacchino, P. Falferi, U. Gambardella, C. Gatti, G. Iannone, *et al.*, Axion search with a quantum-limited ferromagnetic haloscope, *Phys. Rev. Lett.* **124**, 171801 (2020).
- [34] C. Gatti, D. Alesini, D. Babusci, C. Braggio, G. Carugno, N. Crescini, D. Di Gioacchino, P. Falferi, G. Lamanna, C. Ligi, *et al.*, The klash proposal: Status and perspectives, [arXiv:1811.06754](https://arxiv.org/abs/1811.06754) (2018).
- [35] D. Alesini, D. Babusci, F. Björkeröth, F. Bossi, P. Ciambione, G. D. Monache, D. Di Gioacchino, P. Falferi, A. Gallo, C. Gatti, *et al.*, Klash conceptual design report, [arXiv:1911.02427](https://arxiv.org/abs/1911.02427) (2019).
- [36] A. Caldwell, G. Dvali, B. Majorovits, A. Millar, G. Raffelt, J. Redondo, O. Reimann, F. Simon, F. Steffen, M. W. Group, *et al.*, Dielectric haloscopes: a new way to detect axion dark matter, *Phys. Rev. Lett.* **118**, 091801 (2017).
- [37] T. M. collaboration, S. Knirck, J. Schütte-Engel, S. Beurthey, D. Breitmoser, A. Caldwell, C. Diaconu, J. Diehl, J. Egge, M. Esposito, A. Gardikiotis, E. Garutti, S. Heyminck, F. Hubaut, J. Jochum, P. Karst, M. Kramer, C. Krieger, D. Labat, C. Lee, X. Li, A. Lindner, B. Majorovits, S. Martens, M. Matyssek, E. Öz, L. Planat, P. Pralavorio, G. Raffelt, A. Ranadive, J. Redondo, O. Reimann, A. Ringwald, N. Roch, J. Schaffran, A. Schmidt, L. Shtembari, F. Steffen, C. Strandhagen, D. Strom, I. Usherov, and G. Wieching, Simulating madmax in 3d: requirements for dielectric axion haloscopes, *Journal of Cosmology and Astroparticle Physics* **2021** (10), 034.
- [38] M. Lawson, A. J. Millar, M. Pancaldi, E. Vitagliano, and F. Wilczek, Tunable axion plasma haloscopes, *Phys. Rev. Lett.* **123**, 141802 (2019).
- [39] A. J. Millar, S. M. Anlage, R. Balafendiev, P. Belov, K. van Bibber, J. Conrad, M. Demarteau, A. Droster, K. Dunne, A. G. Rosso, J. E. Gudmundsson, H. Jackson, G. Kaur, T. Klaesson, N. Kowitt, M. Lawson, A. Leder, A. Miyazaki, S. Morampudi, H. V. Peiris, H. S. Røising, G. Singh, D. Sun, J. H. Thomas, F. Wilczek, S. Withington, and M. Wooten, *Alpha: Searching for dark matter with plasma haloscopes* (2022).
- [40] A. J. Millar, S. M. Anlage, R. Balafendiev, P. Belov, K. van Bibber, J. Conrad, M. Demarteau, A. Droster, K. Dunne, A. G. Rosso, J. E. Gudmundsson, H. Jackson, G. Kaur, T. Klaesson, N. Kowitt, M. Lawson, A. Leder, A. Miyazaki, S. Morampudi, H. V. Peiris, H. S. Røising, G. Singh, D. Sun, J. H. Thomas, F. Wilczek, S. Withington, M. Wooten, J. Dilling, M. Febbraro, S. Knirck, and C. Marvinney (Endorsers), Searching for dark matter with plasma haloscopes, *Phys. Rev. D* **107**, 055013 (2023).
- [41] S. Al Kenany, M. Anil, K. Backes, B. Brubaker, S. Cahn, G. Carosi, Y. Gurevich, W. Kindel, S. Lamoreaux, K. Lehnert, *et al.*, Design and operational experience of a microwave cavity axion detector for the 20–100 μeV range, *Nucl. Instr. Meth. Phys. Res. A* **854**, 11 (2017).
- [42] D. Di Gioacchino, C. Gatti, D. Alesini, C. Ligi, S. Tocci, A. Rettaroli, G. Carugno, N. Crescini, G. Ruoso, C. Braggio, *et al.*, Microwave losses in a dc magnetic field in superconducting cavities for axion studies, *IEEE Trans. App. Sup.* **29**, 1 (2019).
- [43] D. Ahn, O. Kwon, W. Chung, W. Jang, D. Lee, J. Lee, S. W. Youn, D. Youm, and Y. K. Semertzidis, Maintaining high q-factor of superconducting $\text{YBa}_2\text{Cu}_3\text{O}_{7-x}$ microwave cavity in a high magnetic field, [arXiv:1904.05111](https://arxiv.org/abs/1904.05111) (2019).
- [44] D. Alesini, C. Braggio, G. Carugno, N. Crescini, D. D'Agostino, D. Di Gioacchino, R. Di Vora, P. Falferi, U. Gambardella, C. Gatti, *et al.*, High quality factor photonic cavity for dark matter axion searches, *Rev. Sci. Instr.* **91**, 094701 (2020).
- [45] D. Alesini, C. Braggio, G. Carugno, N. Crescini, D. D'Agostino, D. Di Gioacchino, R. Di Vora, P. Falferi, U. Gambardella, C. Gatti, *et al.*, Realization of a high quality factor resonator with hollow dielectric cylinders for axion searches, *Nucl. Instr. Meth. Phys. Res. A* **985**, 164641 (2021).
- [46] R. Di Vora, D. Alesini, C. Braggio, G. Carugno, N. Crescini, D. D'Agostino, D. Di Gioacchino, P. Falferi, U. Gambardella, C. Gatti, G. Iannone, C. Ligi, A. Lombardi, G. Maccarrone, A. Ortolan, R. Pengo, A. Rettaroli, G. Ruoso, L. Taffarello, and S. Tocci, High- q microwave dielectric resonator for axion dark-matter haloscopes, *Phys. Rev. Applied* **17**, 054013 (2022).
- [47] A. Ranadive, M. Esposito, L. Planat, E. Bonet, C. Naud, O. Buisson, W. Guichard, and N. Roch, Kerr reversal in josephson meta-material and traveling wave parametric amplification, *Nature Communications* **13**, 1737 (2022).
- [48] A. Marin, M. Bignotto, M. Bonaldi, M. Cerdonio, P. Falferi, R. Mezzena, G. A. Prodi, G. Soranzo, L. Taffarello, A. Vinante, S. Vitale, and J.-P. Zendri, Noise measurements and optimization of the high sensitivity capacitive transducer of AURIGA, *Classical and Quantum Gravity* **19**, 1991 (2002).
- [49] C. Braggio, G. Cappelli, G. Carugno, N. Crescini, R. Di Vora, M. Esposito, A. Ortolan, L. Planat, A. Ranadive, N. Roch, and G. Ruoso, A haloscope amplification chain based on a traveling wave parametric amplifier, *Review of Scientific Instruments* **93**, 094701 (2022).
- [50] M. S. Turner, Periodic signatures for the detection of cosmic axions, *Phys. Rev. D* **42**, 3572 (1990).
- [51] M. S. Bartlett, Smoothing periodograms from time-series with continuous spectra, *Nature* **161**, 686 (1948).
- [52] L. Di Luzio, M. Giannotti, E. Nardi, and L. Visinelli, *Physics Reports* **870**, 1 (2020).
- [53] B. M. Brubaker, L. Zhong, S. K. Lamoreaux, K. W. Lehnert, and K. A. van Bibber, Haystack axion search analysis procedure, *Phys. Rev. D* **96**, 123008 (2017).
- [54] P. A. Zyla *et al.*, Review of Particle Physics, (Particle Data Group), *Prog. Theor. Exp. Phys.* **2020**, 10.1093/ptep/ptaa104 (2020), 083C01, <https://academic.oup.com/ptep/article-pdf/2020/8/083C01/34673722/ptaa104.pdf>.
- [55] J. E. Kim, Weak-interaction singlet and strong CP invariance, *Phys. Rev. Lett.* **43**, 103 (1979).
- [56] M. Shifman, A. Vainshtein, and V. Zakharov, Can confinement ensure natural cp invariance of strong interactions?, *Nuclear Physics B* **166**, 493 (1980).
- [57] C. O'Hare, [cajohare/axionlimits: Axionlimits](https://cajohare.github.io/AxionLimits/), <https://cajohare.github.io/AxionLimits/> (2020).
- [58] G. Cowan, K. Cranmer, E. Gross, and O. Vitells, Power-constrained limits, [arXiv:1105.3166](https://arxiv.org/abs/1105.3166) (2011).
- [59] C. Bartram, T. Braine, R. Cervantes, N. Crisosto, N. Du, G. Leum, P. Mohapatra, T. Nitta, L. J. Rosenberg,

G. Rybka, J. Yang, J. Clarke, I. Siddiqi, A. Agrawal, A. V. Dixit, M. H. Awida, A. S. Chou, M. Hollister, S. Knirck, A. Sonnenschein, W. Wester, J. R. Gleason, A. T. Hipp, S. Jois, P. Sikivie, N. S. Sullivan, D. B. Tanner, E. Lentz, R. Khatiwada, G. Carosi, C. Cisneros, N. Robertson, N. Woollett, L. D. Duffy, C. Boutan, M. Jones, B. H. LaRoque, N. S. Oblath, M. S. Taub-

man, E. J. Daw, M. G. Perry, J. H. Buckley, C. Gaikwad, J. Hoffman, K. Murch, M. Goryachev, B. T. McAllister, A. Quiskamp, C. Thomson, M. E. Tobar, V. Bolkhovsky, G. Calusine, W. Oliver, and K. Serniak, Dark matter axion search using a josephson traveling wave parametric amplifier, *Review of Scientific Instruments* **94**, 044703 (2023), <https://doi.org/10.1063/5.0122907>.